J|A|C|S COMMUNICATIONS

Published on Web 08/27/2009

$^{13}C-^{13}C$ Correlation Spectroscopy of Membrane-Associated Influenza Virus Fusion Peptide Strongly Supports a Helix-Turn-Helix Motif and Two Turn Conformations

Yan Sun and David P. Weliky*

Department of Chemistry, Michigan State University, East Lansing, Michigan 48824

Received June 24, 2009; E-mail: weliky@chemistry.msu.edu

Enveloped viruses such as influenza virus are surrounded by a membrane, and infection of target cells begins with joining or "fusion" of viral and host cell membranes into a single membrane.[1] Although membrane fusion is thermodynamically allowed, there is a high kinetic barrier to the fusion process. For this reason, enveloped viruses contain "fusion protein" which catalyzes membrane fusion. For influenza virus, hemagglutinin (HA) is the fusion protein and consists of HA1 and HA2 subunits. The ~20 residues of the HA2 N-teminus are known as the influenza fusion peptide (IFP) and play a critical role in fusion. IFP is initially buried within HA while the influenza virus is endocytosed into the target cell. The low pH of the endosome (~5) triggers a conformational change of HA, and the IFP is exposed and binds to the endosomal membrane with consequent fusion between the viral and endosomal membranes. This paper focuses on the IFP in the absence of the remaining fusion protein. The peptide with IFP sequence serves as a good model system to understand the role of the IFP in influenza viral fusion as evidenced by IFP-induced lipid vesicle fusion at low pH and by the strong correlation between mutation−activity relationships of IFP-induced vesicle fusion and HA-catalyzed cell membrane fusion.[2] IFP is also an important system for developing and testing different simulation methods for membrane-associated peptides.[3−7] It is therefore necessary to have high-resolution structural information for the membrane-associated IFP.

Structures of detergent-associated IFP have been determined by liquid-state NMR and, at pH 5.0, showed an N-terminal helix from residues 2−10 followed by a turn followed by a C-terminal helix from residues 13−18 and, at pH 7.4, showed an N-terminal helix from residues 2−9 followed by a turn and C-terminal extended structure.[8] In membranes, there is substantial experimental support for the N-terminal helical structure and much less support for the turn and C-terminal structure.[2,8−10] Molecular dynamics simulations on membrane-associated IFP from different groups have had conflicting results with observation of helix-turn-helix structure as well as continuous helical structure without a turn.[5−7] In the present work, the conformation of the putative turn region in membrane-associated IFP has been probed with solid-state NMR spectroscopy. The significance of this study is highlighted by observation of IFP-induced fusion between membrane vesicles but not between detergent micelles.

IFP has the sequence GLFGAIAGFIENGWEGMIDGGGKKK-KG where the underlined residues represent the HA2 N-terminus and the subsequent residues increase aqueous solubility. IFP-I10E11 was U−^{13}C,^{15}N labeled at Ile-10 and Glu-11 and IFP-N12G13 was U−^{13}C,^{15}N labeled at Asn-12 and Gly-13. Additional IFPs were synthesized with a single ^{13}CO label or a single ^{13}CO and a single ^{15}N label and are described in the Supporting Information (SI). The solid-state NMR samples contained 0.8 μmol of IFP, 16 μmol of DTPC lipid, and 4 μmol of DTPG lipid and were hydrated with buffer. $^{13}C-^{13}C$ correlation spectra were generated with proton-driven spin diffusion (PDSD) using 10 ms of exchange which led to observation of only intraresidue crosspeaks.[9]

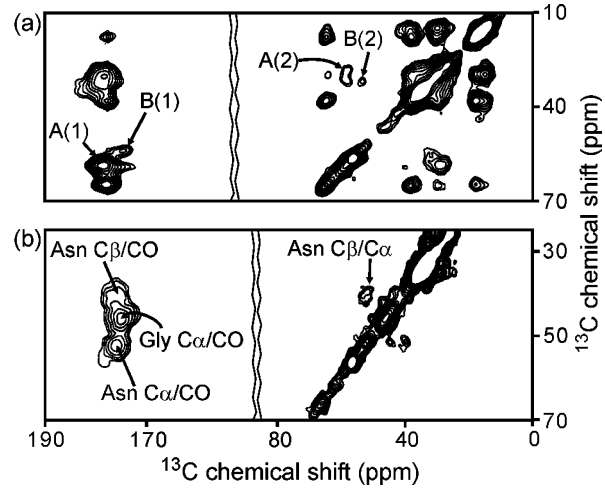

Figure 1. NMR spectra of membrane-associated (a) IFP-I10E11 and (b) IFP-N12G13 at pH 5.0. Some of the peak assignments are shown using the convention f_1 (vertical axis)/f_2 (horizontal axis). The A and B labels represent two distinct sets of Glu-11 crosspeaks: A(1) and B(1), Glu-11 Cα/CO; A(2) and B(2), Glu-11 Cβ/Cα.

Figure 1 displays PDSD spectra of membrane-associated IFP-I10E11 and IFP-N12G13 at fusogenic pH 5.0. The peaks were assigned based on the characteristic chemical shifts of the amino acid spin systems, and Table 1 lists the ^{13}C shifts. Two distinct sets of crosspeaks were observed for Glu-11, and the ratio of intensities of the two peak sets A/B is ~3:1. Backbone dihedral angles were derived from a TALOS program-based analysis of the ^{13}C chemical shifts obtained from the Figure 1 spectra and from spectra of membrane-associated IFP which was either singly ^{13}CO labeled or U−^{13}C,^{15}N labeled from residues 1 through 10.[9,11] The Ile-10 to Gly-13 angles are listed in Table 1, and the Gly-1 to Phe-9

Table 1. ^{13}C Chemical Shifts in ppm and Dihedral Angles in degrees for IFP-I10E11 and IFP-N12G13 Samples at pH 5.0

		CO	Cα	Cβ	Cγ	Cδ	$\varphi/\psi^{c,d}$	$\varphi/\psi^{d,e}$
I10		178.0	65.1	38.2	30.0, 17.9[a]	15.2	−64/−42	−70/−34
E11	A	178.7	58.8	28.9	37.2	181.9[b]	−69/−26	
	B	174.5	54.0	32.0	37.9			−126/156
N12		175.5	51.4	39.8	175.0		−96/8	−113/125
G13		174.5	45.8				87/10	87/10

[a] γ-CH_2 and γ-CH_3 respectively. [b] Chemical shift of COO^-. [c] Dihedral angles corresponding to shift set A of E11. [d] The average uncertainty is ±13°, and specific uncertainties are given in the SI based on distributions of TALOS results. [e] Dihedral angles corresponding to shift set B of E11.

10.1021/ja905198q CCC: $40.75

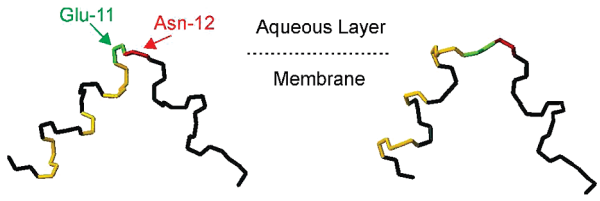

Figure 2. Backbone structures of membrane-associated IFP based on (left) Glu-11 shift set A or (right) Glu-11 shift set B. Glu-11 is in green, Asn-12 is in red, and the hydrophobic residues Leu-2, Phe-3, Ile-6, Phe-9, and Ile-10 are in gold. The structures are drawn from the perspective of "inverted V" membrane insertion with the membrane normal along the symmetry axis of the V and the lipid/water interface near Glu-11 and Asn-12. An alternate view is shown in the SI.

angles are provided in the SI. Figure 2 displays two backbone structures based on these angles and correlated with the A and B crosspeaks in Figure 1. The Trp-14 to Gly-20 dihedral angles in both structures were obtained from the pH 5.0 IFP structures in detergent micelles and were supported by the solid-state NMR observation of helical structure in this region of membrane-associated IFP at both pH 5.0 and pH 7.4; cf. SI.[8] In both the A and B structures, the membrane-associated IFP adopts a helix-turn-helix conformation. Detection of two distinct turn conformations at pH 5.0 is supported by (1) Glu-11 A and B shifts which respectively correlate with canonical shifts of helical and β strand conformations; (2) Asn-12 shifts that do not correlate with helical conformation; (3) solid-state NMR measurement of a 3.6 Å Phe-9 ^{13}CO-Gly-13 ^{15}N distance that agrees quantitatively with the distance in the A structure (cf. SI); and (4) interpretation of ESR spectra of spin-labeled IFP.[12,13] The B crosspeaks are only present for samples at more fusogenic lower pH and are absent for samples at less fusogenic pH 7.4, Figure 3. At pH 7.4, the A/B population ratio is $\geq$10 as estimated from the signal-to-noise of the A crosspeaks. The B conformation may not have been observed in detergent structures because of rapid motional averaging between the A and B structures. The B structure may be correlated with increased fusion at pH 5.0 through the hypothesized "inverted V" insertion of IFP into the membrane, Figure 2.[8] Consider the reasonable hypothesis that the fusion rate is correlated with membrane insertion of the IFP and the resulting membrane perturbation. Membrane insertion would be favored for the pH 5.0 B structure because of the placement of the N-terminal hydrophobic residues on the outside of the V shape in contact with the hydrophobic region of the membrane. In addition to functional relevance, observation of two distinct local conformations in a small membrane-associated peptide is of fundamental interest and the structures provide important data for development of simulation methods that can in principle detect the full IFP conformational distribution.[6,7]

Glu-11, for which two shift sets were observed, is critical for HA2-mediated fusion and for the pH dependence of IFP-mediated vesicle fusion.[14,15] The protonation state of the side chain of Glu-11 was probed as a function of pH through its Cδ shift and relied on the downfield shift of COO$^-$ relative to COOH, Figure 3. The Glu-11 Cγ/Cδ(COO$^-$) crosspeak was absent at pH 4.0, became apparent at pH 5.0, and was strong at pH 7.4. Increasing pH also showed a concurrent decrease in intensity in the region containing the Cγ/Cδ(COOH) crosspeak. This pH dependence in membranes correlates with the Glu-11 pK_a of 5.9 in detergent and suggests that the Glu-11 side chain has contact with water which is consistent with the inverted V membrane location model.[16] The structures in Figure 2 suggest a connection between Glu-11 side chain protonation and formation of the B structure: the charged Glu-11 COO$^-$ side chain in the A structure points toward the aqueous layer, whereas the uncharged COOH in the B structures points toward the membrane interior. The protonation information from Figure 3 will be useful for molecular dynamics studies of the membrane-associated IFP for which protonation states are input parameters.[6]

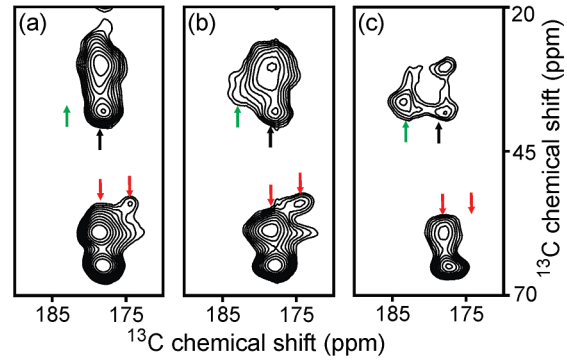

Figure 3. NMR spectra of membrane-associated IFP-UI10E11 at (a) pH 4.0; (b) pH 5.0; and (c) pH 7.4. Green arrows point to the Glu Cγ/Cδ(COO$^-$) crosspeak. This crosspeak is absent at pH 4.0. Black arrows point to the Glu Cγ/Cδ(COOH) crosspeak which is overlapped with other crosspeaks. Red arrows point to crosspeaks of Glu Cα/CO A (left) and B (right). The B crosspeak is absent at pH 7.4.

In summary, solid-state NMR spectra strongly support a helix-turn-helix motif for the membrane-associated IFP at both more fusogenic pH 5.0 and less fusogenic pH 7.4 and a second turn conformation at pH 5.0 which correlates with protonation of the Glu-11 side chain. The NMR results provide insight into the pH dependence of IFP fusion activity and are overall consistent with inverted V membrane location of IFP. The IFP is an important system for testing simulation methods for membrane-associated peptides, and the NMR structures provide significant constraints for this method development.

Acknowledgment. This work was supported by NIH Award AI47153.

Supporting Information Available: Descriptions of experiments and additional experimental data and analysis. This information is available free of charge via the Internet at http://pubs.acs.org.

References

(1) White, J. M.; Delos, S. E.; Brecher, M.; Schornberg, K. *Crit. Rev. Biochem. Mol. Biol.* **2008**, *43*, 189–219.
(2) Nieva, J. L.; Agirre, A. *Biochim. Biophys. Acta* **2003**, *1614*, 104–115.
(3) Huang, Q.; Chen, C. L.; Herrmann, A. *Biophys. J.* **2004**, *87*, 14–22.
(4) Vaccaro, L.; Cross, K. J.; Kleinjung, J.; Straus, S. K.; Thomas, D. J.; Wharton, S. A.; Skehel, J. J.; Fraternali, F. *Biophys. J.* **2005**, *88*, 25–36.
(5) Lague, P.; Roux, B.; Pastor, R. W. *J. Mol. Biol.* **2005**, *354*, 1129–1141.
(6) Sammalkorpi, M.; Lazaridis, T. *Biochim. Biophys. Acta* **2007**, *1768*, 30–38.
(7) Jang, H.; Michaud-Agrawal, N.; Johnston, J. M.; Woolf, T. B. *Proteins: Struct., Funct., Bioinform.* **2008**, *72*, 299–312.
(8) Han, X.; Bushweller, J. H.; Cafiso, D. S.; Tamm, L. K. *Nat. Struct. Biol.* **2001**, *8*, 715–720.
(9) Bodner, M. L.; Gabrys, C. M.; Struppe, J. O.; Weliky, D. P. *J. Chem. Phys.* **2008**, *128*, 052319.
(10) Macosko, J. C.; Kim, C. H.; Shin, Y. K. *J. Mol. Biol.* **1997**, *267*, 1139–1148.
(11) Cornilescu, G.; Delaglio, F.; Bax, A. *J. Biomol. NMR* **1999**, *13*, 289–302.
(12) Zhang, H. Y.; Neal, S.; Wishart, D. S. *J. Biomol. NMR* **2003**, *25*, 173–195.
(13) Lai, A. L.; Tamm, L. K. *J. Biol. Chem.* **2007**, *282*, 23946–23956.
(14) Korte, T.; Epand, R. F.; Epand, R. M.; Blumenthal, R. *Virology* **2001**, *289*, 353–361.
(15) Lai, A. L.; Park, H.; White, J. M.; Tamm, L. K. *J. Biol. Chem.* **2006**, *281*, 5760–5770.
(16) Chang, D. K.; Cheng, S. F.; Lin, C. H.; Kantchev, E. A. B.; Wu, C. W. *Biochim. Biophys. Acta* **2005**, *1712*, 37–51.

JA905198Q

Supporting Information of "^{13}C–^{13}C Correlation Spectroscopy of Membrane-Associated Influenza Virus Fusion Peptide Strongly Supports a Helix-Turn-Helix Motif and Two Turn Conformations" by Yan Sun and David P. Weliky

1. Peptide synthesis

U-^{13}C,^{15}N-Glycine, U-^{13}C,^{15}N-Isoleucine, *N*-Fmoc-δ-*O*-*t*-butyl-U-^{13}C,^{15}N-Glutamic Acid, and α-*N*-Fmoc-γ-*N*-trityl-U-^{13}C,^{15}N-Asparagine were purchased from Cambridge Isotope Laboratories, Andover, MA. Isoleucine and glycine were 9-fluorenylmethoxycarbonyl (Fmoc)-protected using literature procedures.[1,2] The sequence of IFP is GLFGAIAGFIENGWEGMIDGGGKKKKG and was synthesized using Fmoc chemistry. The underlined part is the 20 N-terminal residues of the influenza A X31 strain HA2 fusion protein and the non-native glycines and lysines increased aqueous solubility. IFP was cleaved from the resin for 2-3 hours using a mixture of trifluoroacetic acid:thioanisole:1,2-ethanedithiol:anisole in a 90:4:4:2 volume ratio. Trifluoroacetic acid was removed from the cleavage filtrate with nitrogen gas and IFP was precipitated with cold *t*-butyl methyl ether. IFP was purified by reversed-phased high performance liquid chromatography using a semi-preparative C18 column and a water-acetonitrile gradient. Mass spectroscopy was used for peptide identification.

2. Solid-state NMR sample preparation

Some of the vesicle samples were made with 1-palmitoyl-2-oleoyl-*sn*-glycero-3-phosphocholine (POPC)/1-palmitoyl-2-oleoyl-*sn*-glycero-3-[phospho-*rac*-(1-glycerol)] (POPG) lipids in a 4:1 mol ratio. The other samples were made with 1,2-di-*O*-tetradecyl-*sn*-glycero-3-phosphocholine (DTPC)/1,2-di-*O*-tetradecyl-*sn*-glycero-3-[phospho-*rac*-(1-glycerol)] (DTPG) in a 4:1 mol ratio. The POPC:POPG mixture has a liquid-crystalline to gel phase transition temperature of -2 ^{o}C and the DTPC:DTPG mixture has a liquid-crystalline to gel phase transition

near ambient temperature.[3,4] The reason for the major PC fraction in both mixtures was the significant quantity of phosphatidylcholine lipids in membranes of host epithelial cells of the influenza virus.[5] Incorporation of the minor PG fraction was based on the small quantity of negatively charged lipids in these membranes. In addition, PC/PG mixtures of this approximate composition have been previously used in structural and functional studies of IFP and HA2.[6-12]

The sample preparation protocol began with dissolution in chloroform of lipids (20 μmol total). The chloroform was removed under a stream of nitrogen followed by overnight vacuum pumping. The lipid film was suspended in 2 mL aqueous buffer (10 mM HEPES/5 mM MES) at pH 5.0 or pH 7.4 and was homogenized with ten freeze-thaw cycles. Large unilamellar vesicles were formed by extrusion through a 100 nm diameter polycarbonate filter (Avestin, Ottawa, ON). Quantitation of IFP was done using A_{280} with $\varepsilon_{280} = 5700\ cm^{-1}\ M^{-1}$. IFP (0.8 μmol) was easily dissolved in 2 mL aqueous buffer solution at pH 5.0 or pH 7.4, and the IFP solution was then added to the vesicle solution. The IFP/vesicle mixture was gently vortexed overnight and then ultracentrifuged at 150000*g* for five hours. There was quantitative membrane binding of IFP as evidenced by $A_{280} < 0.01$ in the supernatant and by calculation using the experimental binding constants.[8] The membrane pellet with associated bound IFP was transferred to a 4 mm diameter magic angle spinning (MAS) NMR rotor. The pH of the hydrated pellet was confirmed before and after the NMR experiments by testing with pH paper. Four different samples were made for each labeled IFP, with two samples at pH 5.0 and two at pH 7.4. For each pH, one sample had POPC/POPG membranes and the other one had DTPC/DTPG membranes. The IFP-I10E11/DTPC/DTPG sample at pH 4.0 was made from the corresponding sample initially prepared at pH 5.0. After obtaining the NMR spectrum, the sample was re-suspended in buffer at pH 5.0, the pH was reduced to 4.0 with hydrochloric acid, the sample was ultracentrifuged, and

the IFP-I10E11/membrane pellet at pH 4.0 was transferred to a MAS rotor.

3. Solid-state NMR spectroscopy

Experiments were done on a 9.4 T solid-state NMR spectrometer (Varian Infinity Plus, Palo Alto, CA) using a MAS probe in double resonance $^{13}C/^{1}H$ configuration. The ^{13}C and ^{1}H frequencies were 100.8 and 400.8 MHz respectively. The ^{13}C shifts were externally referenced to the methylene resonance of adamantane at 40.5 ppm which allows direct comparison with ^{13}C shift databases derived from liquid-state NMR assignments of proteins.[13-15] These databases are appropriate for solid-state NMR data as evidenced by similar ^{13}C shifts observed for the same protein in either aqueous solution or the microcrystalline state.[16-18] The proton-driven spin diffusion (PDSD) pulse sequence contained an initial ^{1}H $\pi/2$ pulse followed by a ^{1}H-^{13}C cross polarization (CP), an evolution period t_1, a ^{13}C $\pi/2$ pulse that rotated the ^{13}C transverse magnetization to the longitudinal axis, a spin diffusion period τ during which ^{13}C magnetization was mixed among nearby nuclei, a second ^{13}C $\pi/2$ pulse that rotated the ^{13}C magnetization back to the transverse plane, and a detection period t_2. A ~70 KHz ^{1}H decoupling field with two-pulse phase modulation was applied during t_1 and t_2, but not during τ.[19] The following parameters were typical for PDSD experiments: 10 kHz MAS frequency, 50 kHz ^{1}H $\pi/2$ pulse, 36-42 kHz ramp on the ^{13}C CP rf field, 56 kHz ^{1}H CP rf field, 50 kHz ^{13}C $\pi/2$ pulse, 25 μs t_1 dwell time, 200 t_1 values, 20 μs t_2 dwell time, 256 t_2 points, 10 ms exchange time, and 1 s recycle delay. Hypercomplex data were obtained by acquiring two individual FIDs for each t_1 point with either a ^{13}C $(\pi/2)_x$ or $(\pi/2)_y$ pulse at the end of the t_1 evolution period. Spectra were processed with NMRPipe software using 200 Hz Gaussian line broadening in each dimension.[20] The ratio of intensities between adjacent contours was typically 1.3.

4. NMR spectra of membrane-associated IFP

The full PDSD spectra in Fig. S1, S2a,d and S3c correspond to the spectra in Fig. 1a, 3c,a and 1b in the main text, respectively. Because of MAS and radiofrequency heating, the sample temperature was at least a few degrees above the cooling gas temperatures, so the membranes in the DTPC/DTPG and POPC/POPG samples were respectively in the frozen gel and unfrozen liquid-crystalline phases. For a particular pH, similar peak shifts and relative intensities were observed for samples containing either DTPC/DTPG or POPC/POPG, cf. Fig S1 and S2c, Fig. S2a and b, Fig. S3a and b, and Fig. S3c and d. This result is consistent with IFP turn structure that is independent of membrane phase and correlates with N-terminal helical structure which is also independent of membrane phase.[6] Both shift sets A and B are present in the spectra of all of the IFP-I10E11 samples at pH 5.0 or pH 4.0. Only shift set A was observed in spectra of all IFP-I10E11 samples at pH 7.4. Neglecting this difference, the peak shifts and relative intensities were similar for samples at pH 5.0 and 7.4. Assignments were based on intra-residue correlation and on characteristic amino acid-type shifts and were complete in the sense that all of the peaks of significant intensity were assigned. The uncertainty in a peak shift was ±0.5 ppm as determined by comparison of different spectra and f_1/f_2 and f_2/f_1 crosspeaks.

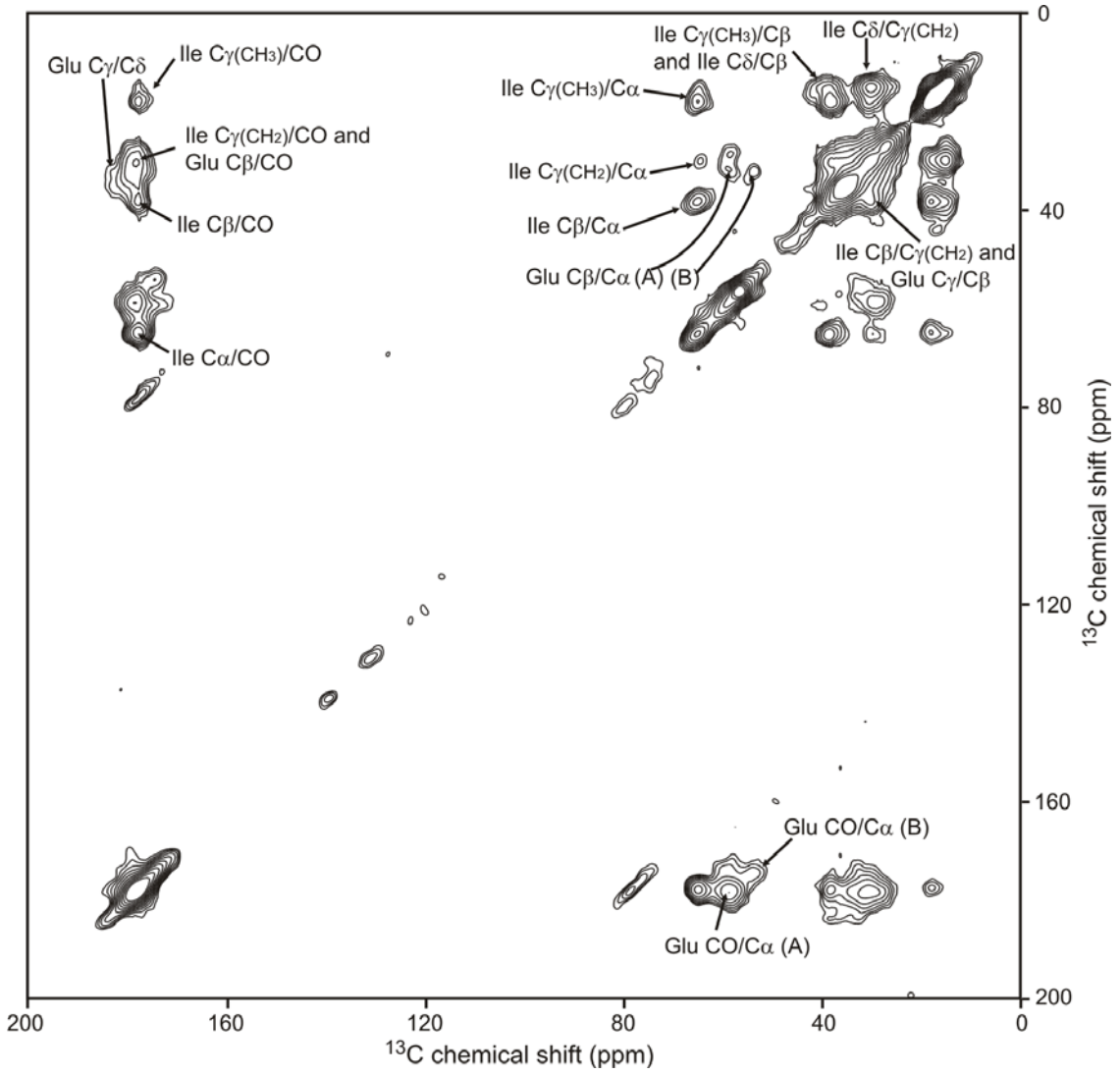

Figure S1. PDSD spectrum for DTPC/DTPG-associated IFP-I10E11 at pH 5.0 and cooled by nitrogen gas at –50 ^{o}C. The data were collected with 10 ms exchange time and total signal averaging time of ~1.5 days. Peak assignments are listed using the convention of assignment in f_1 (vertical axis)/f_2 (horizontal axis).

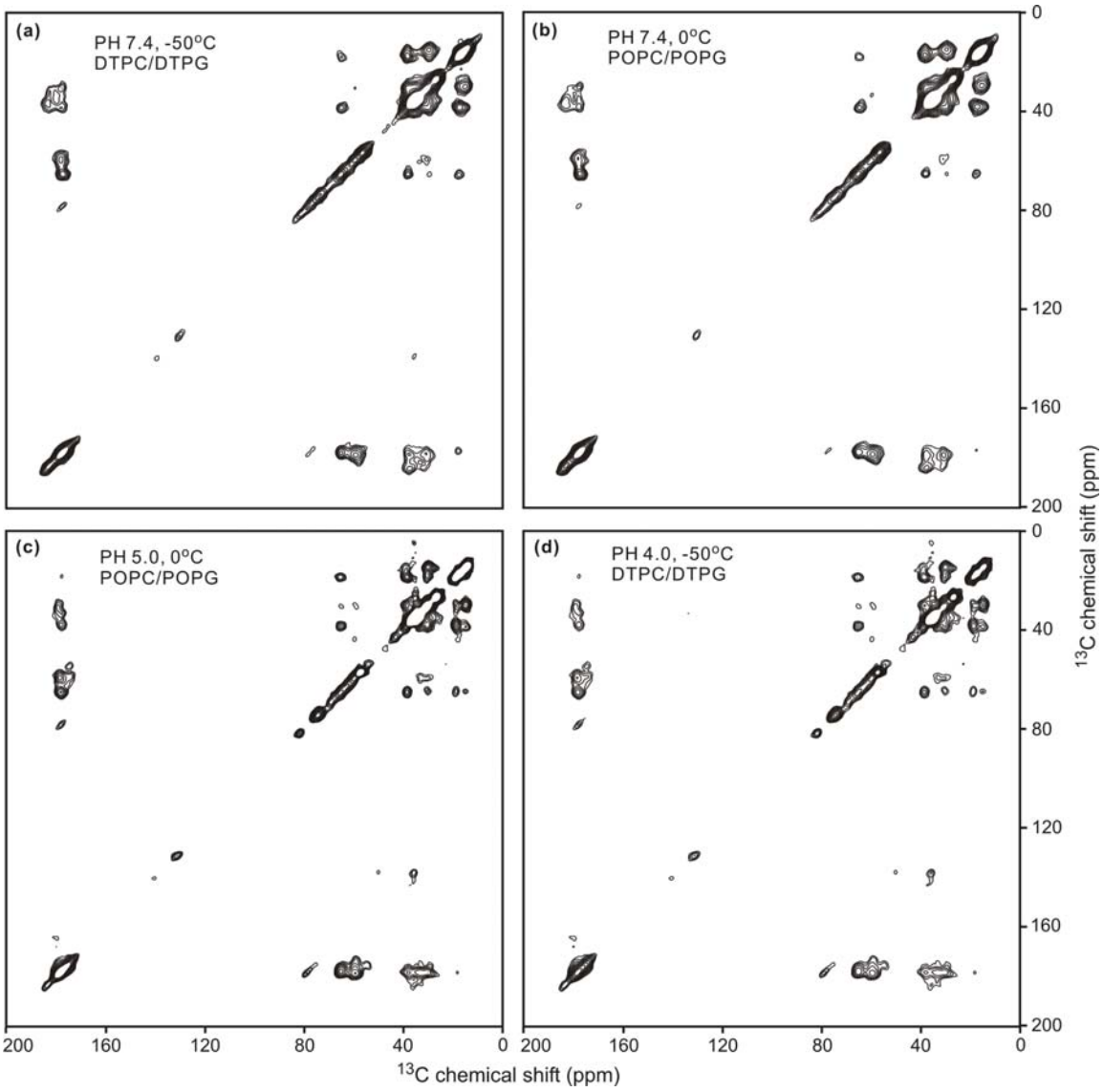

Figure S2. PDSD spectra for membrane-associated IFP-I10E11. Each spectrum was collected with 10 ms exchange time and total signal averaging time of (a-c) ~1.5 days or (d) ~2.5 days. The listed temperatures are for the cooling gas.

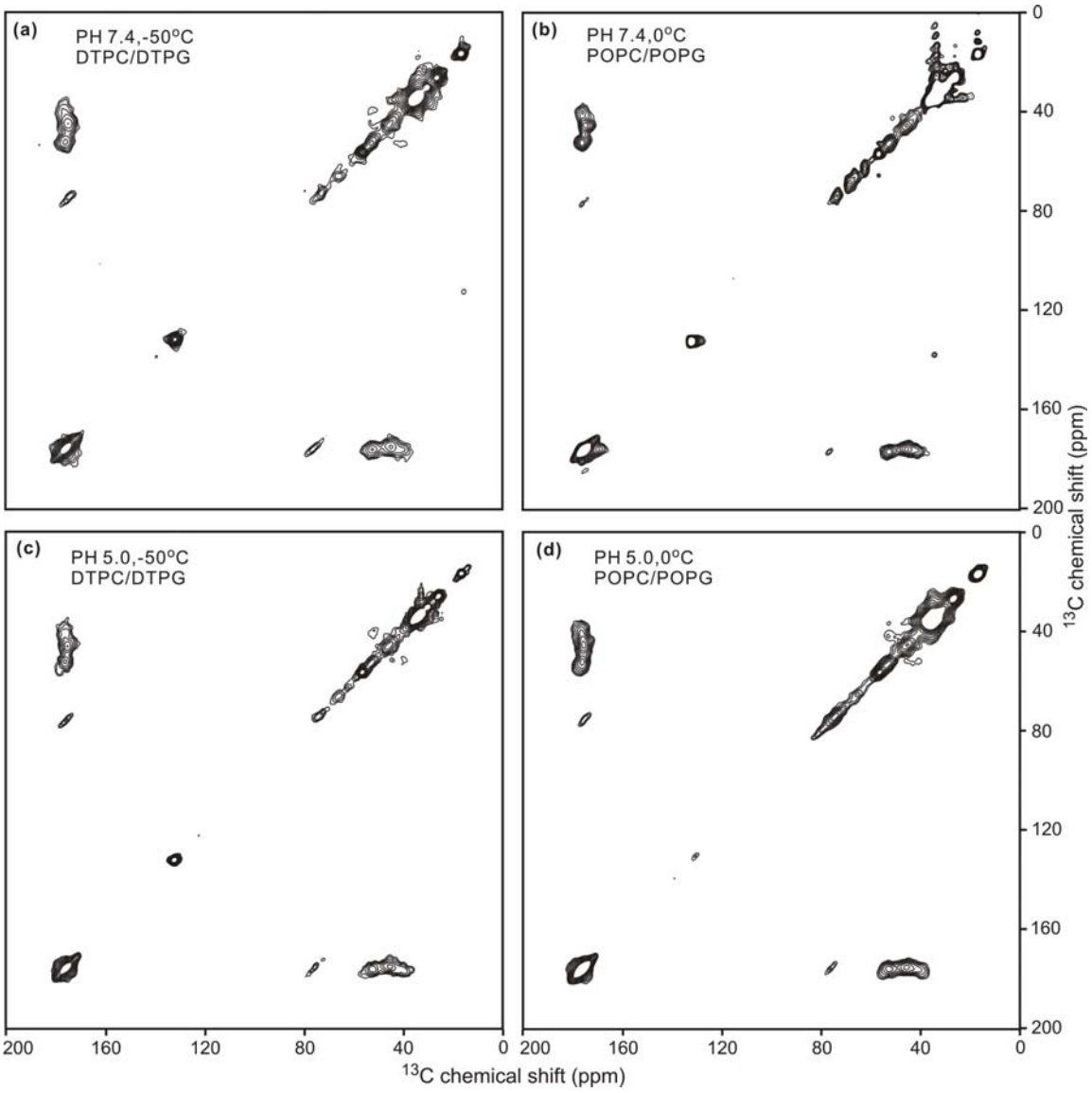

Figure S3. PDSD spectra for membrane-associated IFP-N12G13. Each spectrum was collected with 10 ms exchange time and total signal averaging time of ~1.5 days. The listed temperatures are for the cooling gas.

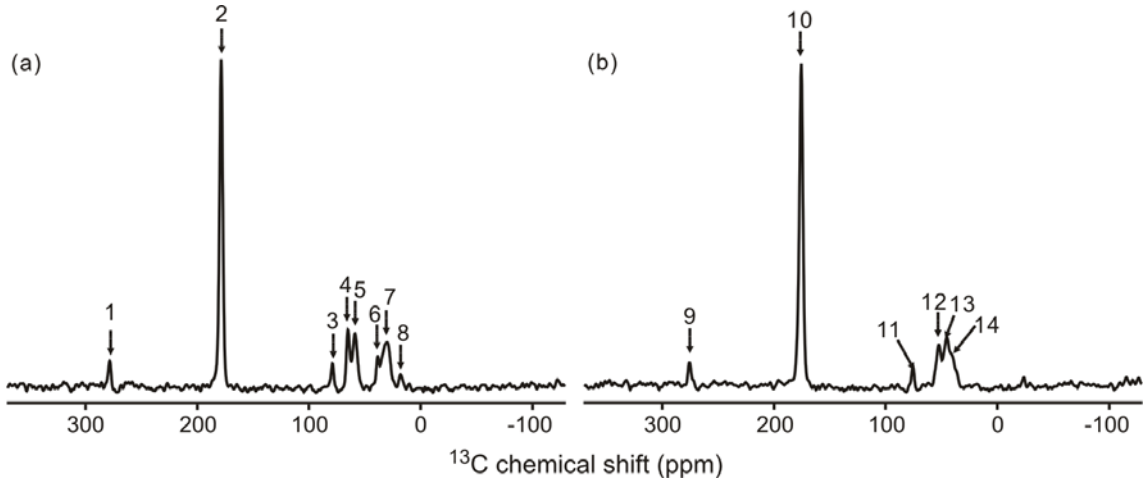

Figure S4. 1D slices along the f_2 dimension from (a) Fig. 1a in the main text with f_1 = 178.0 ppm which is the shift of Ile-10 CO and (b) Fig. 1b in the main text with f_1 = 175.5 ppm which is the shift of Asn-12 CO. The assignments of the peaks are: 1, 3, 9 and 11, spinning sidebands; 2, overlap of Ile CO/Glu CO/Glu Cδ; 4, Ile Cα; 5, Glu Cα; 6, Ile Cβ; 7, overlap of Glu Cγ/Ile Cγ–CH_2/Glu Cβ; 8, overlap of Ile Cδ/Ile Cγ–CH_3; 10, overlap of Asn CO/Gly CO/Asn Cγ; 12, Asn Cα; 13, Gly Cα; and 14, Asn Cβ.

5. Chemical shifts and dihedral angle prediction

Dihedral angles were generated by the TALOS program using the measured ^{13}CO, ^{13}Cα and ^{13}Cβ chemical shifts.[13] The Ile-10, Glu-11, Asn-12, and Gly-13 shifts are listed in Table 1 in the main text and the ^{13}CO shifts in ppm of other residues were obtained from selectively-labeled IFP samples: Gly-1, 171.2; Phe-3, 178.1; Ala-5, 179.5; Ala-7, 179.3; Gly-8, 175.4; and Phe-9, 178.6.[21] The remaining shifts were based on previously obtained 2D correlation spectra of a membrane-associated IFP sample at pH 5.0 with U-^{13}C,^{15}N labeling over the first ten residues.[12] The Leu-2 and Ile-6 shifts obtained from this spectrum were unambiguous while a single set of chemical shifts was observed for both Ala-5 and Ala-7 and another single set was observed for

Phe-3 and Phe-9. For glycines in this sample, four sets of CO/Cα crosspeaks were observed: (1) 175.9/47.4; (2) 176.1/41.0; (3) 170.6/43.6; and (4) 170.0/46.4 ppm. The Gly-1 CO shift of 171.2 ppm led to consideration of shift sets (3) and (4) for Gly-1 but the different shift sets had minor effect on the predicted dihedral angles, i.e. predicted values from one set were within the range of standard deviations of the values from the other set. Table S1 was generated using the 43.6 ppm Cα shift for Gly-1. For Gly-4 and Gly-8, only shift set (1) was considered because these shifts were more consistent with helical structure which is supported by chemical shifts in the N-terminal region and by the 4.0 Å Ala-5 ^{13}CO ··· Phe-9 ^{15}N distance determined by solid-state NMR.[12,15,21-23]

The φ and ψ angles in Table S1 are the averages of the best matches predicted by the TALOS program. Residues Leu-2 through Phe-9 and Gly-13 have dihedral angles independent of the Glu-11 chemical shifts. Residues Ile-10, Glu-11 and Asn-12 have different φ and ψ angles corresponding to the A and B Glu-11 chemical shift sets.

Table S1. Backbone dihedral angles in degrees for membrane-associated IFP at pH 5.0 and detergent-associated IFP.[9] Uncertainties are in the parentheses.

	Membrane-associated IFP				Detergent-associated IFP			
					pH 5.0		pH 7.4	
	φ		ψ		φ	ψ	φ	ψ
Gly-1	ND [a]		ND		ND	-160 (1)	ND	154 (4)
Leu-2	-59 (2) [b]		-33 (8) [b]		-47 (1)	-44 (1)	-56 (1)	-49 (1)
Phe-3	-63 (8)		-38 (12)		-52 (2)	-35 (1)	-64 (0.1)	-46 (1)
Gly-4	-64 (7)		-42 (7)		-67 (1)	-35 (3)	-53 (1)	-51 (1)
Ala-5	-66 (3)		-37 (7)		-72 (2)	-36 (3)	-62 (1)	-40 (1)
Ile-6	-68 (5)		-45 (5)		-58 (1)	-41 (1)	-64 (0.1)	-63 (1)
Ala-7	-62 (6)		-40 (8)		-66 (1)	-35 (5)	-57 (2)	-31 (3)
Gly-8	-62 (8)		-39(6)		-54 (5)	-52 (6)	-63 (3)	-53 (2)
Phe-9	-67 (5)		-37 (8)		-61 (5)	-44 (4)	-53 (3)	-30 (3)
	Shift set A		Shift set B					
	φ	ψ	φ	ψ				
Ile-10	-63 (5)	-42 (7)	-70 (11)	-34 (13)	-49 (3)	-32 (10)	-66 (4)	-14 (4)
Glu-11	-69 (11) [c]	-27 (13) [c]	-126 (29)	156 (13)	-98 (13)	-2.5 (4)	-121 (7)	5 (4)
Asn-12	-96 (13)	8 (12)	-113 (18) [b]	125 (27) [b]	-137 (24)	34 (39)	-146 (6)	52 (63)
Gly-13	87 (11) [d]	10 (9) [d]	87 (9) [d]	10 (11) [d]	130 (53)	5 (15)	119 (73)	7 (6)
Trp-14					-40 (3)	-42 (4)	-48 (9)	-123 (83)
Glu-15					-53 (4)	-33 (4)	-103 (52)	12 (80)
Gly-16					-70 (6)	-18 (9)	-121 (76)	-19 (23)
Met-17	ND		ND		-98 (11)	-11 (4)	-113 (22)	-2 (10)
Ile-18					-71 (6)	-46 (9)	-88 (18)	-1 (46)
Asp-19					-42 (46)	151 (77)	-85 (56)	110 (66)
Gly-20					78 (67)	ND	-116 (83)	ND

[a] ND ≡ not determined.
Number of TALOS matches used to determine dihedral angles and uncertainties are [b] 9; [c] 8; [d] 7. For all other residues in the membrane-associated IFP, 10 matches were used.

Table S1 also lists the dihedral angles for detergent-associated IFP based on 20 low energy structures. The dihedral angles of residues Leu-2 through Ile-10 for both membrane-

associated and detergent-associated IFPs at both pHs are consistent with each other and with α helical structure. There are similar Gly-13 dihedral angles within error for membrane-associated and detergent-associated IFP. For membrane-associated IFP, residues Glu-11 and Asn-12 have distinct dihedral angles corresponding to shift sets A and B of Glu-11. The Glu-11 A and B angles respectively correlate with helical and β strand conformation while the Asn-12 B angles correlate with β strand conformation and the A angles correlate with irregular conformation. The Glu-11 and Asn-12 A angles are most consistent, although not within error, with the pH 5.0 detergent values, while the B angles are not consistent with the detergent values at either pH. This work highlights the ability of solid-state NMR to detect multiple peptide structures.[24,25]

A qualitative check on the TALOS-derived angles of Glu-11 and Asn-12 is comparison of the experimental CO, Cα, and Cβ shifts to the corresponding shift distributions derived from a shift database of proteins of known structure.[15] The A Glu-11 CO, Cα, and Cβ shifts of 178.7, 58.8, and 28.9 ppm are more consistent with the helical shift distributions of 178.6 ± 1.2, 59.1 ± 1.2, and 29.4 ± 1.0 ppm than with β strand distributions of 175.4 ± 1.4, 55.5 ± 1.7, and 32.0 ± 2.0 ppm. In some contrast, the B Glu-11 shifts of 174.5, 54.0, and 32.0 ppm are more consistent with β strand shifts. The experimental Asn-12 shifts of 175.5, 51.4, and 39.8 ppm are less consistent with the helical distributions of 176.9 ± 1.6, 55.5 ± 1.4, and 38.6 ± 1.3 ppm and more consistent with the β strand distributions of 174.6 ± 1.7, 52.7 ± 1.5, and 40.1 ± 2.0 ppm. This latter correlation is consistent with the break in regular helical conformation in a helix-turn-helix structure.

6. IFP structural models

The structures were generated using the MOLMOL program and for residues Leu-2 to Gly-13, the solid-state NMR-derived angles in Table S1 were used.[26] For membrane-associated

IFP, a Gly-16 ^{13}CO shift of 175.2 ppm has been measured in selectively labeled samples and is invariant to pH and consistent with helical structure.[15,21] At both pH 5.0 and 7.4, solid-state NMR measurement of a 4.5 Å Gly-13 ^{13}CO···Met-17 ^{15}N distance was also consistent with C-terminal helical structure.[21] For detergent-associated IFP, the C-terminal region has helical conformation at pH 5.0 and extended conformation at pH 7.4 so for Trp-14 to Gly-20 as well as Gly-1, dihedral angles from detergent-associated IFP at pH 5.0 were used to generate the IFP

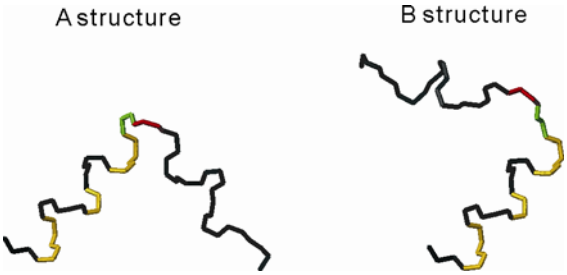

structures.

Figure S5. Alternate view of the B structure created from alignment of the N-terminal helix with the A structure.

7. Phe-9 ^{13}CO···Gly-13 ^{15}N distance

Fig. S6 displays solid-state NMR rotational-echo double-resonance (REDOR) data and fitting of the labeled IFP Phe-9 ^{13}CO···Gly-13 ^{15}N distance at pH 5.0 and pH 7.4.[22] The REDOR data rely on the "Δ*S*" difference in ^{13}CO signal between "S_0" and "S_1" spectra where ^{13}CO signals in the S_1 spectrum are attenuated because of dipolar coupling to nearby ^{15}N nuclei. The dipolar coupling is proportional to (distance)$^{-3}$ and the ^{13}CO···^{15}N distance can be determined from fitting of the "normalized dephasing" $\Delta S/S_0$ as a function of dipolar evolution or dephasing

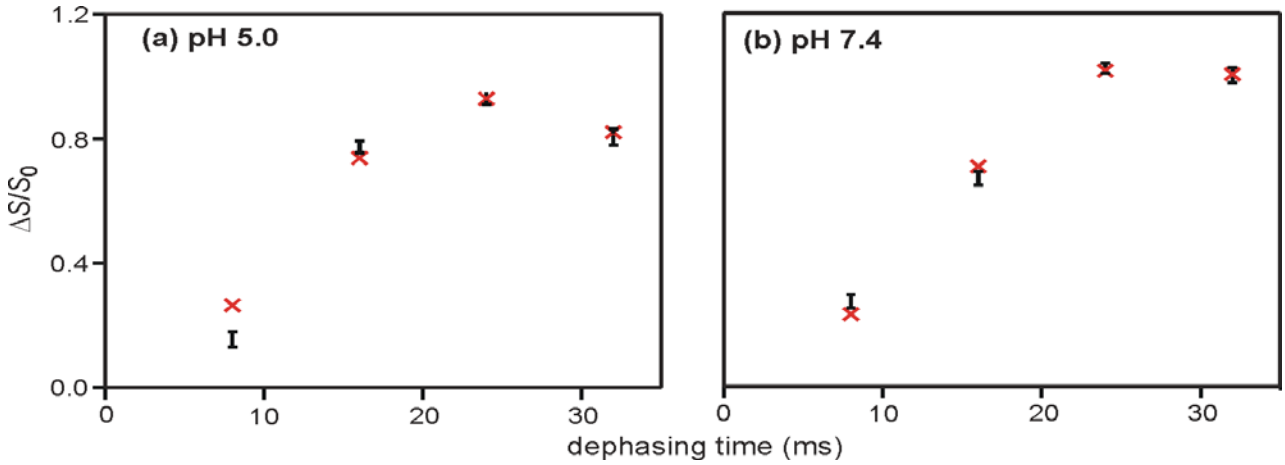

Figure S6. Solid-state NMR REDOR experimental data (vertical black lines with error bars) and best-fit simulations (red crosses) of DTPC/DTPG-associated IFP at (a) pH 5.0 and (b) pH 7.4. Samples were prepared as described in sections 1 and 2 and IFP was ^{13}CO labeled at Phe-9 and ^{15}N labeled at Gly-13.

time, Fig. S6. Details of the REDOR experiments and fitting have been described previously.[27,28] At pH 7.4 at long dephasing times, $\Delta S/S_0 \approx 1$, which indicates that nearly all of the Phe-9 ^{13}COs are close to the Gly-13 ^{15}Ns. At pH 5.0 at the corresponding dephasing times, $\Delta S/S_0 < 1$, which indicates that there are two populations of Phe-9 ^{13}COs, one close to Gly-13 ^{15}N nuclei with population "f" and one further away from ^{15}N nuclei with population of $1 - f$. These populations respectively correlate with the A and B structures in Fig. 2 in the main text for which the Phe-9 ^{13}CO···Gly-13 ^{15}N distances are 3.7 and 8.1 Å and with the conclusion that there is only appreciable population of the B structure at pH 5.0. Because there are only four data points, fitting was done with two parameters, f and structure A Phe-9 ^{13}CO···Gly-13 ^{15}N distance, with the reasonable assumption that the B structure contribution to $\Delta S/S_0$ is ≈ 0 because of the long distance and the small value of $1 - f$. The best-fit f and distance are 1.00 ± 0.03 and 3.7 ± 0.1 Å

at pH 7.4 and 0.89 ± 0.03 and 3.5 ± 0.1 Å at pH 5.0. The best-fit Phe-9 $^{13}CO\cdots$Gly-13 ^{15}N distances at both pHs are shorter than the 4.1 Å distance of regular α helical structure and are consistent with the 3.7 Å distance in the turn in the A structure.[9] These REDOR analyses qualitatively support the pH dependence of the population of the B structure although the fractional population at pH 5.0 is somewhat less than that deduced from the 2D crosspeak intensities.

8. IFP mutant experiments

Solid-state NMR constant-time double-quantum buildup with finite pulses (fp-CTDQBU) experiments are a good approach to determine inter-residue ^{13}C-^{13}C distances which are straightforwardly correlated to backbone dihedral angles.[27,29,30] This approach was specifically targeted to measurement of the Glu-11 $^{13}CO\cdots$Asn-12 ^{13}CO distance because it is geometrically related to the Asn-12 φ angle and this angle has non-helical values in all of the structures in Table S1. Analysis of fp-CTDQBU data is most straightforward and accurate for an isolated ^{13}CO-^{13}CO spin pair; i.e. for IFP that contains two ^{13}CO labels. Because protected ^{13}CO labeled Glu and Asn were not commercially available, we made a IFP-E11V,N12A mutant with ^{13}CO labeling at Val-11 and Ala-12.[31,32] The global structure of this mutant IFP was assessed by a IFP-E11V,N12A mutant with a ^{13}CO label at Ala-5 and a ^{15}N label at Phe-9. The data were compared to the wild-type IFP with the same labeling scheme. For the wild-type and mutant IFPs, REDOR S_0 and S_1 spectra at 24 ms dephasing time are displayed, Fig. S7. For wild-type IFP, the Ala-5 CO chemical shift of 179.5 ppm was more consistent with the 179.4 ± 1.3 ppm distribution of Ala CO shifts in helical conformation and less consistent with the 176.1 ± 1.5 ppm distribution in β strand conformation.[15] Relative to the S_0 spectrum, the large reduction in signal intensity in the S_1 spectrum was consistent with close proximity of the Ala-5 ^{13}CO and Phe-9 ^{15}N nuclei and

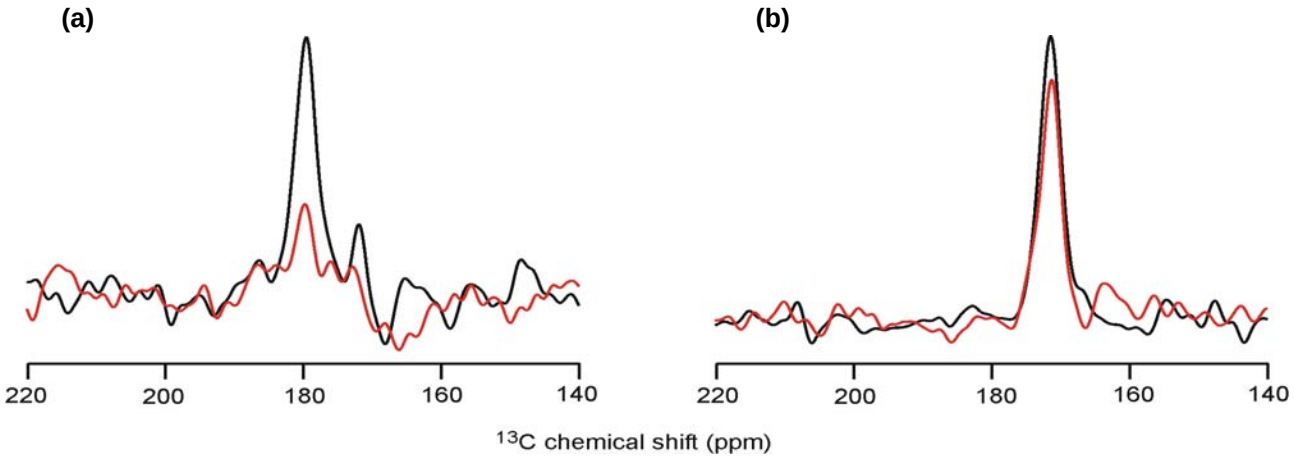

Figure S7. Solid-state NMR REDOR S_0 (black) and S_1(red) spectra for DTPC/DTPG-associated (a) wild-type IFP and (b) IFP-E11V,N12A mutant that were ^{13}CO labeled at Ala-5 and ^{15}N labeled at Phe-9. Samples were prepared as described in sections 1 and 2, the dephasing time was 24 ms, and the numbers of scans summed for each spectrum were (a) 24974 and (b) 35840.

analysis of the $\Delta S/S_0$ of this and other dephasing times resulted in a best-fit Ala-5 ^{13}CO···Phe-9 ^{15}N distance of 4.1 Å which was the expected value for α helical structure. In some contrast, the IFP-E11V,N12A mutant had a Ala-5 ^{13}CO shift of 172.0 ppm and the $\Delta S/S_0$ were much smaller than those in the wild-type IFP. Both observations were consistent with a large change in the mutant from the global helical structure of wild-type IFP and showed that this mutant IFP was not a reasonable structural model for wild-type IFP. This result also highlights that Glu-11 is a critical IFP residue as stated and referenced in the main text.

9. References

(1) Chang, C. D.; Waki, M.; Ahmad, M.; Meienhofer, J.; Lundell, E. O.; Haug, J. D. *Int. J. Peptide Protein Research* **1980**, *15*, 59-66.
(2) Lapatsanis, L.; Milias, G.; Froussios, K.; Kolovos, M. *Synthesis* **1983**, *8*, 671-673.
(3) Silvius, J. R., Thermotropic Phase Transitions of Pure Lipids in Model Membranes and Their Modification By Membrane Proteins. In *Lipid-Protein Interactions*, Jost, P. C.; Griffith, O. H., Eds. John Wiley & Sons: New York, 1982; Vol. 2, pp 239-281.

(4) Caffrey, M. *LIPIDAT: a database of thermodynamic data and associated information on lipid mesomorphic and polymorphic transitions*, CRC: Boca Raton, 1993.
(5) Worman, H. J.; Brasitus, T. A.; Dudeja, P. K.; Fozzard, H. A.; Field, M. *Biochemistry* **1986**, *25*, 1549-1555.
(6) Bodner, M. L.; Gabrys, C. M.; Parkanzky, P. D.; Yang, J.; Duskin, C. A.; Weliky, D. P. *Magn. Reson. Chem.* **2004**, *42*, 187-194.
(7) Macosko, J. C.; Kim, C. H.; Shin, Y. K. *J. Mol. Biol.* **1997**, *267*, 1139-1148.
(8) Han, X.; Tamm, L. K. *Proc. Natl. Acad. Sci. U.S.A.* **2000**, *97*, 13097-13102.
(9) Han, X.; Bushweller, J. H.; Cafiso, D. S.; Tamm, L. K. *Nature Struct. Biol.* **2001**, *8*, 715-720.
(10) Wasniewski, C. M.; Parkanzky, P. D.; Bodner, M. L.; Weliky, D. P. *Chem. Phys. Lipids* **2004**, *132*, 89-100.
(11) Curtis-Fisk, J.; Preston, C.; Zheng, Z. X.; Worden, R. M.; Weliky, D. P. *J. Am. Chem. Soc.* **2007**, *129*, 11320-11321.
(12) Bodner, M. L.; Gabrys, C. M.; Struppe, J. O.; Weliky, D. P. *J. Chem. Phys.* **2008**, *128*, 052319.
(13) Cornilescu, G.; Delaglio, F.; Bax, A. *J. Biomol. NMR* **1999**, *13*, 289-302.
(14) Morcombe, C. R.; Zilm, K. W. *J. Magn. Reson.* **2003**, *162*, 479-486.
(15) Zhang, H. Y.; Neal, S.; Wishart, D. S. *J. Biomol. NMR* **2003**, *25*, 173-195.
(16) Igumenova, T. I.; Wand, A. J.; McDermott, A. E. *J. Am. Chem. Soc.* **2004**, *126*, 5323-5331.
(17) Franks, W. T.; Zhou, D. H.; Wylie, B. J.; Money, B. G.; Graesser, D. T.; Frericks, H. L.; Sahota, G.; Rienstra, C. M. *J. Am. Chem. Soc.* **2005**, *127*, 12291-12305.
(18) Marulanda, D.; Tasayco, M. L.; Cataldi, M.; Arriaran, V.; Polenova, T. *J. Phys. Chem. B* **2005**, *109*, 18135-18145.
(19) Bennett, A. E.; Rienstra, C. M.; Auger, M.; Lakshmi, K. V.; Griffin, R. G. *J. Chem. Phys.* **1995**, *103*, 6951-6958.
(20) Delaglio, F.; Grzesiek, S.; Vuister, G. W.; Zhu, G.; Pfeifer, J.; Bax, A. *J. Biomol. NMR* **1995**, *6*, 277-293.
(21) Sun, Y. Ph. D. Thesis, Michigan State University, East Lansing, 2009.
(22) Gullion, T.; Schaefer, J. *J. Magn. Reson.* **1989**, *81*, 196-200.
(23) Balbach, J. J.; Yang, J.; Weliky, D. P.; Steinbach, P. J.; Tugarinov, V.; Anglister, J.; Tycko, R. *J Biomol NMR* **2000**, *16*, 313-27.
(24) Petkova, A. T.; Leapman, R. D.; Guo, Z. H.; Yau, W. M.; Mattson, M. P.; Tycko, R. *Science* **2005**, *307*, 262-265.
(25) Buffy, J. J.; Traaseth, N. J.; Mascioni, A.; Gor'kov, P. L.; Chekmenev, E. Y.; Brey, W. W.; Veglia, G. *Biochemistry* **2006**, *45*, 10939-10946.
(26) Koradi, R.; Billeter, M.; Wuthrich, K. *J. Molec. Graph.* **1996**, *14*, 51-55.
(27) Zheng, Z., Yang, R., Bodner, M.L., and Weliky, D.P. *Biochemistry* **2006**, *45*, 12960-12975.
(28) Qiang, W.; Weliky, D. P. *Biochemistry* **2009**, *48*, 289-301.
(29) Ishii, Y. *J. Chem. Phys.* **2001**, *114*, 8473-8483.
(30) Zheng, Z.; Qiang, W.; Weliky, D. P. *Magn. Reson. Chem.* **2007**, *245*, S247-S260.
(31) Lai, A. L.; Park, H.; White, J. M.; Tamm, L. K. *J. Biol. Chem.* **2006**, *281*, 5760-5770.
(32) Korte, T.; Epand, R. F.; Epand, R. M.; Blumenthal, R. *Virology* **2001**, *289*, 353-361.